DIFFRACTION CONTRAST FROM DISSOCIATED FRANK DISLOCATIONS

II.* COMPARISON OF EXPERIMENTAL AND COMPUTED ELECTRON MICROGRAPHS

By L. M. CLAREBROUGH† and A. J. MORTON†

[*Manuscript received December* 19, 1968]

Summary

Experimental and computed images for edges of Frank dislocation loops in quenched copper–aluminium alloys and in quenched silver are compared. The comparison shows that Frank dislocations are dissociated in these materials. By matching the computed and experimental images, the degree of dissociation is determined and the stacking fault energy of the various materials is estimated.

I. INTRODUCTION

It has been shown in Part I (present issue, pp. 351–70) that there are many features of the diffraction contrast from dissociated Frank dislocations which are sensitive to the separation of the Shockley and stair-rod dislocations. In this paper, experimental images of Frank dislocation loops in quenched copper–aluminium alloys and in quenched silver are matched with images computed for the experimental values of t, $\boldsymbol{FN}$, $\boldsymbol{B}$, $\boldsymbol{b}$, $\boldsymbol{u}$, $\boldsymbol{g}$, and w (these symbols are defined in Part I). It is shown that Frank dislocation loops in these materials are dissociated. The selection of experimental images given here illustrates most of the major features of contrast from dissociated Frank dislocations discussed in Part I. Further, the image matching has enabled the extent of dissociation to be determined, and thus estimates of the stacking fault energy to be made for the different materials.

II. EXPERIMENTAL

(*a*) *Materials and Quenching Procedure*

The copper–aluminium alloys containing $9\cdot4$ at.% aluminium and $15\cdot6$ at.% aluminium were prepared by melting copper ($99\cdot99$% Cu) and aluminium ($99\cdot99$% Al) in graphite crucibles in an atmosphere of argon. The resulting ingots were homogenized and fabricated into strip in the usual manner. For quenching, specimens 15 cm long, 3 mm wide, and 75 μ thick were heated electrically in an atmosphere of carbon monoxide until a small molten zone appeared and were then quenched into water at 20°C. After quenching, the specimens were aged for 1 hr at 100°C.

The silver, Cominco 69 grade silver ($99\cdot9999$% Ag), was supplied by the Consolidated Mining and Smelting Company of Canada. For quenching, specimens

* Part I, *Aust. J. Phys.*, 1969, **22**, 351–70.

† Division of Tribophysics, CSIRO, University of Melbourne, Parkville, Vic. 3052.

15 cm long, 3 mm wide, and 125 μ thick were heated electrically in an atmosphere of argon until a small molten zone appeared and were then quenched into silicone oil at 20°C.

(*b*) *Nature of the Defects*

The copper–aluminium alloys and the silver contained simple Frank dislocation loops, prismatic loops, complex Frank loops (cf. following paper, present issue pp. 393–419), and stacking fault tetrahedra.

In the present paper, we are only concerned with the simple Frank dislocation loops. The nature of the fault was determined from the bright field images of faulted loops that intersected one or both surfaces of the foil (Loretto 1965). Following Mazey, Barnes, and Howie (1962), the upward drawn normal from a $\langle 213 \rangle$ diffraction pattern was indexed unambiguously as [213] or [123] and the sign of the 111 reflecting vector determined from the sense of rotation from, say, the [213] to the [101] beam direction. This rotation also fixed the plane of the loop and, following Hashimoto, Howie, and Whelan (1962), the sign of $\boldsymbol{g}.\boldsymbol{R}$ (where $\boldsymbol{R}$ is the displacement vector of the fault) was fixed from the nature of the outermost fringe so that, knowing $\boldsymbol{g}$, $\boldsymbol{R}$ is determined. In all cases examined the loops were found to be intrinsically faulted.

(*c*) *Image Computation*

The method of image computation has been described in Part I and the elastic constants used (Hearmon 1956) are given below.

	c_{11}	c_{12}	c_{44}
Silver	12·40	9·34	4·61 (10^{11} dyn cm^{-2})
Copper–aluminium (9·98 at.%)	15·95	11·76	7·66 (10^{11} dyn cm^{-2})

As in Part I, 7% below and 15% above background intensity have been taken as the visibility limits in nearly all cases. However, for matching some experimental images a different scale of grey that involved different visibility limits (Humble 1968) was used, and this is indicated in the appropriate figure legend. In converting the separations of the stair-rod and Shockley dislocations, S, from extinction distances, ξ, to Angstrom units, the extinction distances given by Hirsch *et al.* (1965) were used, the values for copper being used for the copper–aluminium alloys.

III. Results

(*a*) *Copper–Aluminium (9·4 at.%) Alloy*

Figure 1 shows the images of a large Frank loop for the $\bar{1}\bar{1}1$ and $\bar{2}20$ reflections. The loop lies on (111) and CD is the line of intersection of the loop with the top of the foil. For the $\bar{1}\bar{1}1$ reflection there is contrast along the edges of the loop for which

Fig. 1.—Comparison of experimental ($\times 60\,000$) and computed images of a Frank dislocation loop in a copper–aluminium (9·4 at.%) alloy:

$\boldsymbol{FN}$ [9 7 13], $\boldsymbol{u}$ [$\bar{1}$01], $t = 8\xi_{111}$.

The values of S, $\boldsymbol{B}$, $\boldsymbol{g}$, and w are indicated. Line resolution is 42 Å in (*a*) and 28 Å in (*b*).

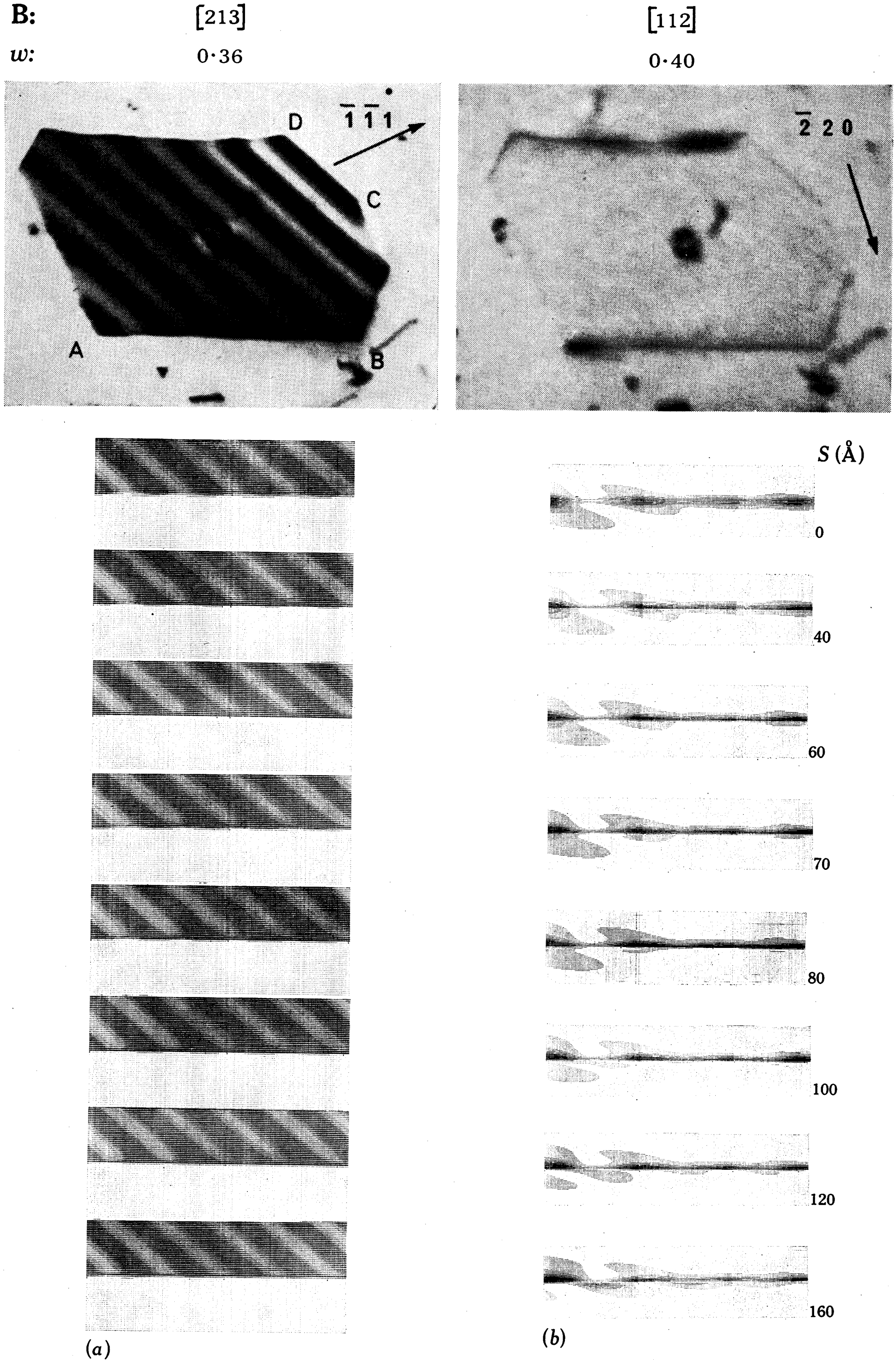
B:
w:
[213]
0·36
[112]
0·40
D
$\bar{1}\,\bar{1}\,1$
C
A
B
$\bar{2}\,2\,0$
S (Å)
0
40
60
70
80
100
120
160
(a)
(b)

Fig. 1

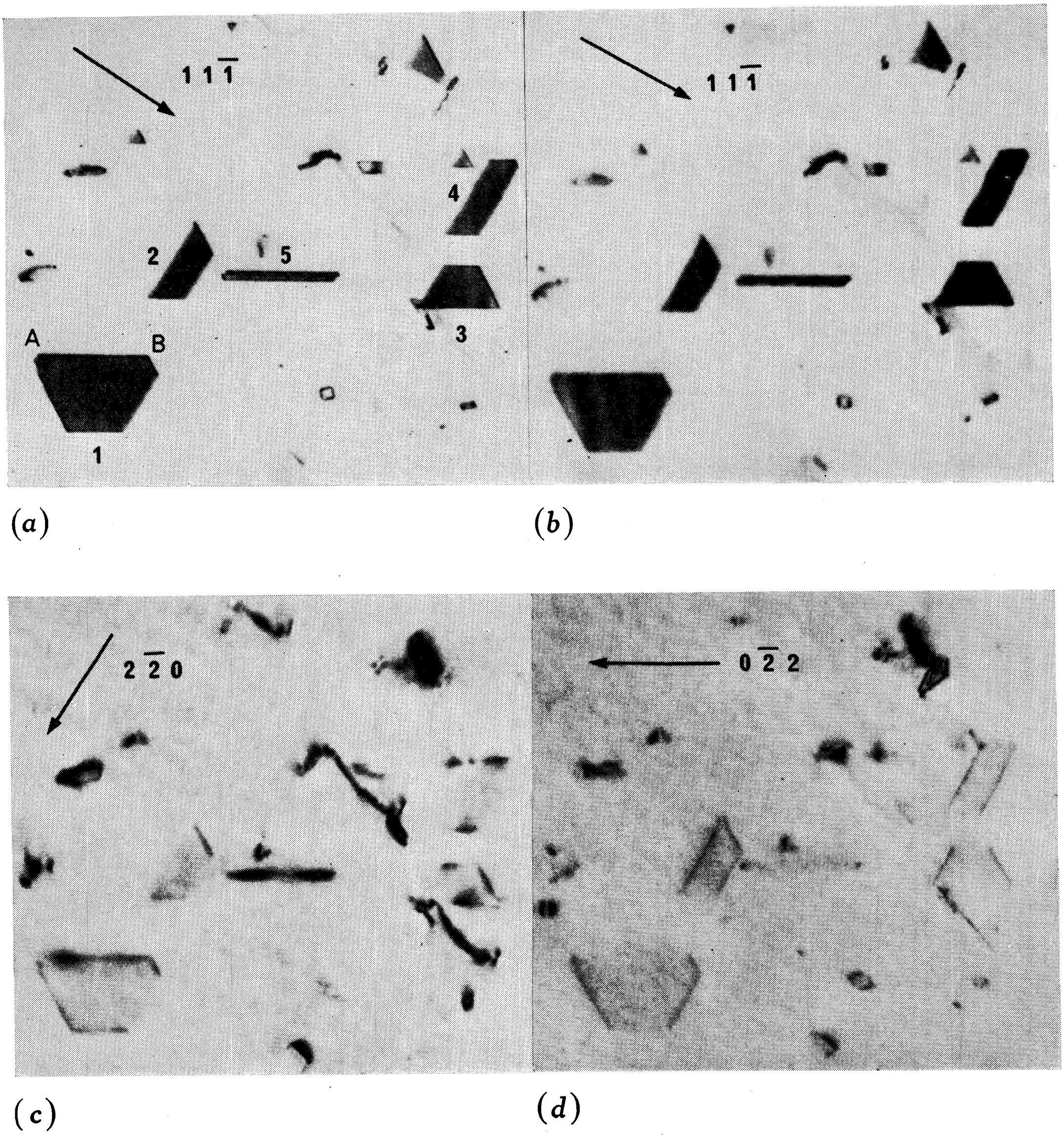

Fig. 2.—Frank dislocation loops in a copper–aluminium (9·4 at.%) alloy (×60 000):

(*a*) ***B*** [549], ***g*** $11\bar{1}$; (*b*) ***B*** [213], ***g*** $11\bar{1}$;

(*c*) ***B*** [112], ***g*** $2\bar{2}0$; (*d*) ***B*** [111], ***g*** $0\bar{2}2$.

$\boldsymbol{g}.\boldsymbol{u} \neq 0$ and no contrast for those edges for which $\boldsymbol{g}.\boldsymbol{u} = 0$. For the $\bar{2}20$ reflection the edges for which $\boldsymbol{g}$ is not parallel to $\boldsymbol{u}$ show strong contrast. The $\bar{2}20$ image shows a slight departure from background intensity in the interior of the loop and very faint contrast along the edges for which $\boldsymbol{g}$ is parallel to $\boldsymbol{u}$. These effects result from having a third weak beam operating.

The computed images in Figure 1 are for the edge AB which is shallowly inclined to the foil surface. It can be seen that the computed images for an undissociated Frank loop along AB do not match the experimental contrast. The $\bar{1}\bar{1}1$ image shows no enhanced contrast along AB in the light fringes and, although the $\bar{2}20$ image shows faint continuous contrast, the strongest features in this image are

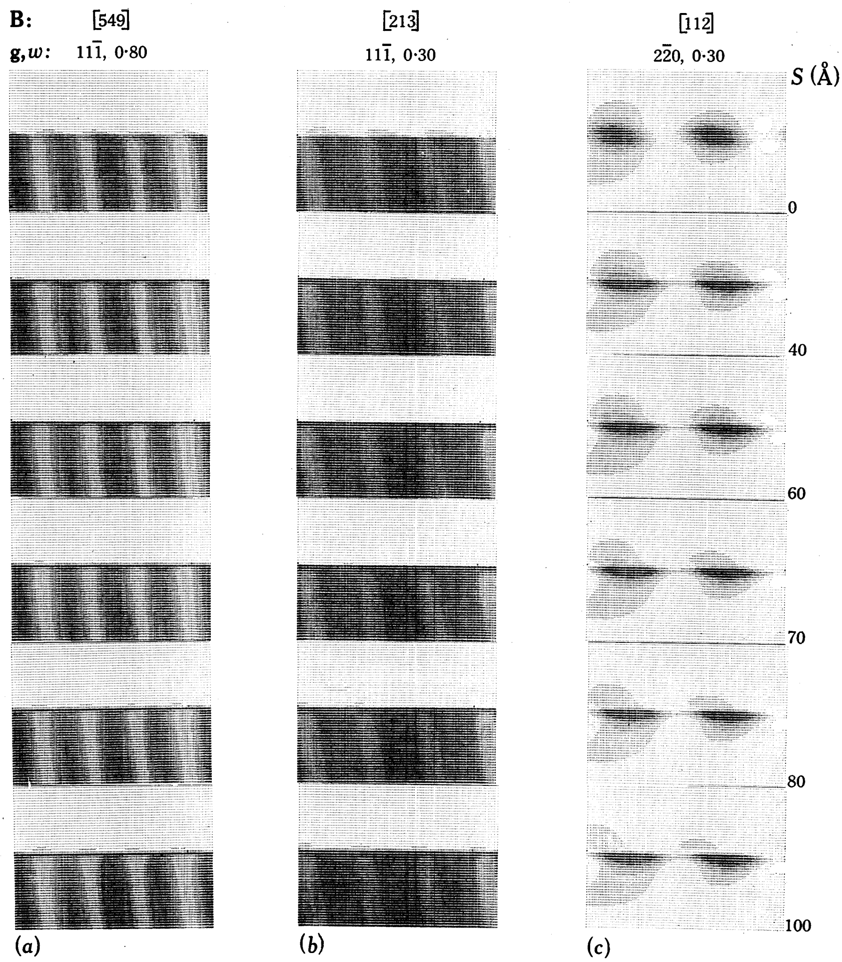

Fig. 3.—Computed images for the edge AB of loop 1 in Figure 2:

$$\boldsymbol{FN}\ [425],\quad \boldsymbol{u}\ [0\bar{1}1],\quad t = 7\xi_{111}.$$

The values of S, $\boldsymbol{B}$, $\boldsymbol{g}$, and w are indicated. Line resolution is 29 Å.

double. However, the images for the dissociated cases are better matches to the experimental images. The $\bar{2}20$ images alone are not very satisfactory for choosing the degree of dissociation, but they do suggest a dissociation of less than 100 Å. The $\bar{1}\bar{1}1$ images indicate that the dissociation is greater than 40 Å and less than 100 Å, since at $S = 40$ Å there is very little contrast in the computed image at the edge of the loop for the second light fringe in from A and for $S = 100$ Å the contrast at the edge of the loop in the first light fringe is too strong. It is considered that the best match of computed and experimental images occurs at $S = 70$ Å.

Figure 2 shows further examples of 111 and 220 contrast. The Frank loops 1, 2, 3, and 4 all lie on (111) and do not intersect the foil surfaces. Loop 5 is a more complex loop. In Figure 2(*a*), $w = 0 \cdot 8$ for the $11\bar{1}$ reflection and, at this large value of w, the fringes tend to fade into the general dark contrast within the loop, but the contrast for those edges of the loops for which $\boldsymbol{g}.\boldsymbol{u} \neq 0$ is strong and continuous; no contrast occurs at the edges for which $\boldsymbol{g}.\boldsymbol{u} = 0$. The fringes are clearer and the contrast at the edges of the loops although less sharp is still continuous for the $11\bar{1}$ reflection at $w = 0 \cdot 3$ (Fig. 2(*b*)). The images of these loops for the $2\bar{2}0$ and $0\bar{2}2$ reflections are given in Figures 2(*c*) and 2(*d*). In all cases the edges of the loops for which $\boldsymbol{g}$ is not parallel to $\boldsymbol{u}$ give continuous rather than double and dotted images for the 220 reflections. Further, there does not appear to be any residual contrast along those edges for which $\boldsymbol{g}$ is parallel to $\boldsymbol{u}$.

It is clear from Figure 3, which gives computed images for the edge AB of loop 1 firstly considered as undissociated and then dissociated to different extents, that the contrast at the edges of these loops is incompatible with undissociated Frank dislocations. Although this loop and that in Figure 1 are in very similar geometrical situations, the edge AB here is more steeply inclined to the foil surface than the edge AB of the loop in Figure 1, resulting in the $2\bar{2}0$ image computed for the undissociated Frank (Fig. 3(*c*)) being clearly double and dotted. This computed image has little resemblance to the experimental image. Further, the $11\bar{1}$ images for the undissociated Frank show no contrast along AB (Figs 3(*a*) and 3(*b*)). Although the comparison of experimental and computed images shows that the dislocation along AB is dissociated, there are no characteristics, in this case, that enable the degree of dissociation to be determined.

As shown in Part I, it is characteristic of the contrast from a dissociated Frank for 220 reflections that features of the image remain on the same side of the dislocation in $+\boldsymbol{g}$ and $-\boldsymbol{g}$. An example of this effect is shown in Figure 4. The loop lies on (111) and intersects both surfaces of the foil, the intersection with the top of the foil being along CD. The dot-like artefact indicated with a small arrow appears in all the images in Figure 4 and should not be confused with the contrast arising from the dislocation. The $0\bar{2}2$ image (Fig. 4(*c*)) shows that the contrast along the dislocations is approximately continuous with the dotted features lying on the fault side of the dislocations. The image of the dislocation AD shows the strongest contrast at the intersection D of the dislocation with the top of the foil, whilst the image for BC is strongest at the intersection B with the bottom of the foil. The intensity of the contrast at the other intersections A and C is above background level. It should be noted that at D and B the strong contrast is on the fault side of the dislocation. Comparison of the $0\bar{2}2$ image with the $02\bar{2}$ images (Figs 4(*a*) and 4(*b*)) shows that on reversing the sense of $\boldsymbol{g}$, although the image inverts from top to bottom of the foil, the dotted features do not invert from side to side of the dislocations, but remain on the fault side. The image is more continuous at large w than at small w, as can be seen by comparing Figure 4(*b*) ($w = 0 \cdot 6$) with Figure 4(*a*) ($w = 0$), and the dotted features of the image are clearer at $w = 0$.

Figure 5 shows computed images for the dislocation AD for the $0\bar{2}2$ and $02\bar{2}$ reflections, for values of S from 0 to 100 Å. The images for the undissociated Frank are double and thus do not fit the experimental images. It is considered that the best agreement between the experimental and computed images is for $S = 60$ Å.

An example of 002 contrast for $\boldsymbol{g}.\boldsymbol{u} = 0$ is given in Figures 6(a) and 6(b). The loop lies on (111), is four-sided, and intersects both surfaces of the foil. For the 200 and $\bar{2}00$ reflections, $\boldsymbol{g}.\boldsymbol{u} = 0$ for the edge AB which intersects the bottom of the foil at B. The contrast along this edge shows a light band between the strong contrast along AB and the fault fringes for the 200 reflection (Fig. 6(a)), and for the $\bar{2}00$ reflection an inner dark line, terminating the fault fringes, is separated by a light band from a dotted image along the edge of the loop. The dotted character of this portion of the image is most pronounced near the surfaces of the foil. The $\bar{1}\bar{1}1$ image (Fig. 6(c)) shows contrast along the edge AB of the loop. The edge of the loop CD shows reversal of contrast in 200 and $\bar{2}00$ in agreement with the results of Part I for dissociated Frank dislocations for which $\boldsymbol{g}.\boldsymbol{u} \neq 0$.

The computed images for the edge AB are also given in Figure 6. Although the 200 and $\bar{2}00$ images of the undissociated Frank show some of the general features of the experimental images, they are not compatible with the fine detail of these images. Further, the $\bar{1}\bar{1}1$ image of the undissociated Frank does not show the contrast found in the experimental image. It is considered that the best match to the experimental images occurs at $S = 80$ Å. Below this value of S the inner dark line terminating the fault fringes for the $\bar{2}00$ reflection is not pronounced and above this value the dotted contrast at the edge of the loop becomes too weak. The computed images for the other reflections match the experimental images at this separation.

The experimental cases considered so far involve overlap of the fault in the Frank loop and the fault resulting from dissociation when viewed in the beam direction (Figs 1–3 and 6) or where the beam direction nearly lies in the plane containing the fault formed by dissociation (Figs 4 and 5). Figures 7 and 8 show an example where dissociation would result in non-overlapping faults. The loop ABCD is on $(1\bar{1}1)$, CD is the intersection with the bottom of the foil, and the edge AB is along [110]. The dissociation of the Frank dislocation along [110] would produce a stacking fault on $(\bar{1}11)$ and this fault and that on $(1\bar{1}1)$ would not overlap for the experimental rotation of the beam direction from [506] to [103] (Figs 7(a) and 7(b)) or from [718] to [213] (Figs 7(c) and 7(d)).

For the [506] beam direction, there is complete reversal of the contrast along AB on changing the operative reflection from $0\bar{2}0$ to 020 (compare Fig. 7(a) with 8(a)). However, for the [103] beam direction there is only partial reversal of the contrast on going from $0\bar{2}0$ to 020, the 020 image still showing streaks of dark contrast crossing the light fringes at the edge of the loop (compare Fig. 7(b) with 8(b)). For the $\bar{1}\bar{1}1$ reflection, the image along AB is weak in the [718] beam direction (Fig. 7(c)) and in the [213] beam direction the fringe angle appears to change close to AB (Fig. 7(d)).

It can be seen from a comparison of the experimental images with the computed images in Figures 7 and 8 that these features of the contrast are due to dissociation of the Frank dislocation along AB. In the [506] and [103] beam directions, the images for the $0\bar{2}0$ reflection (Figs 7(a) and 7(b)) for the undissociated Frank and for the various values of S are similar. However, in contrast to the experimental 020

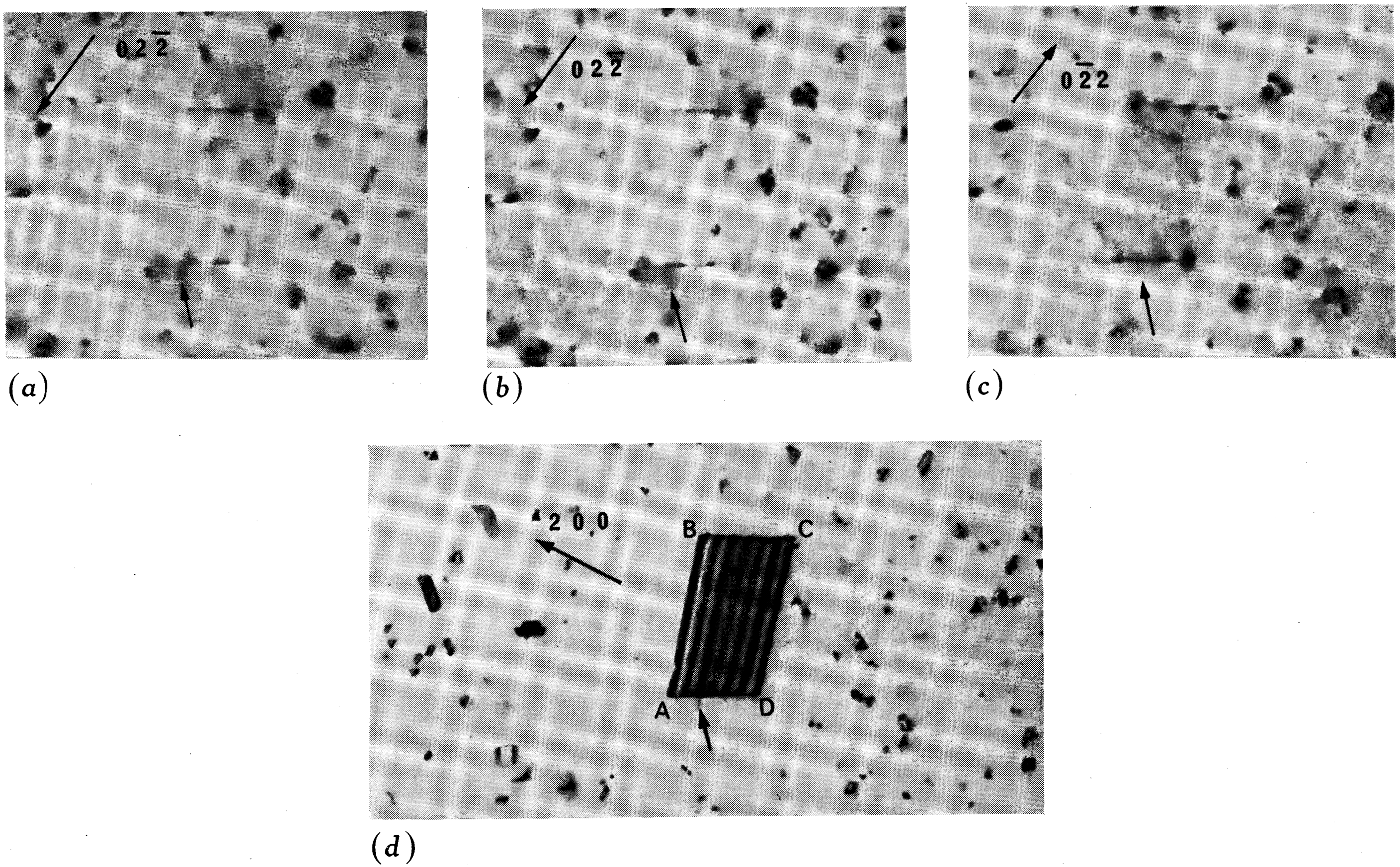

Fig. 4.—Portion of a Frank dislocation loop in a copper–aluminium (9·4 at.%) alloy (×60 000):

(a) $\boldsymbol{B}$ [$\bar{1}$88], $\boldsymbol{g}$ $02\bar{2}$; (b) $\boldsymbol{B}$ [$\bar{1}$88], $\boldsymbol{g}$ $02\bar{2}$; (c) $\boldsymbol{B}$ [$\bar{1}$88], $\boldsymbol{g}$ $0\bar{2}2$;

(d) $\boldsymbol{B}$ [011], $\boldsymbol{g}$ 200.

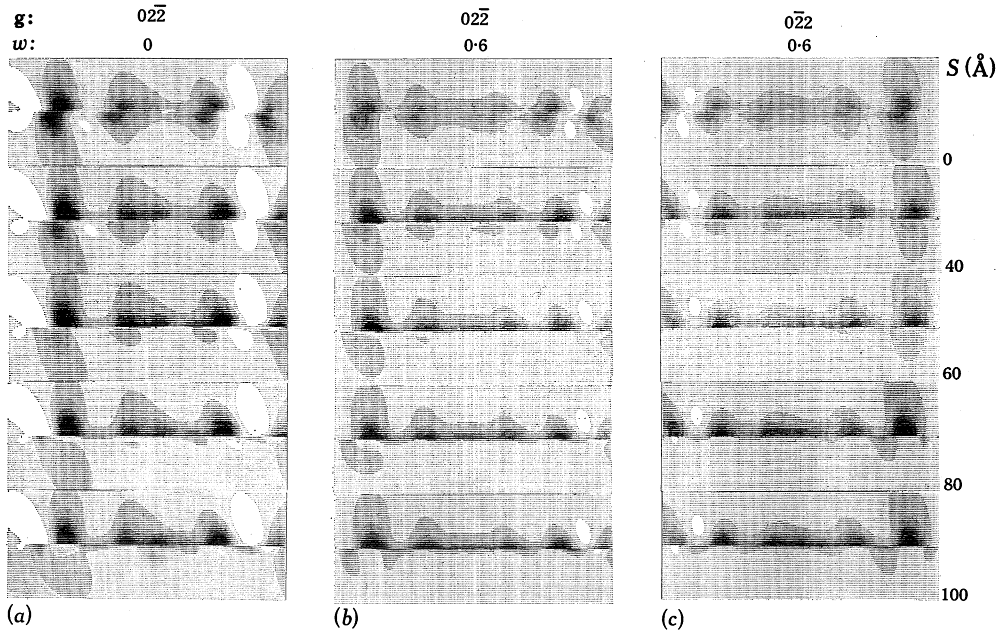

Fig. 5.—Computed images corresponding to the experimental images along AD in Figures 4(*a*), 4(*b*), and 4(*c*):

$\boldsymbol{B}$ [$\bar{1}$88], $\boldsymbol{FN}$ [102], $\boldsymbol{u}$ [$\bar{1}$01], $t = 4\xi_{022}$.

The values of S, $\mathbf{g}$, and w are indicated. Line resolution is 15 Å.

(a)

(b)

(c)

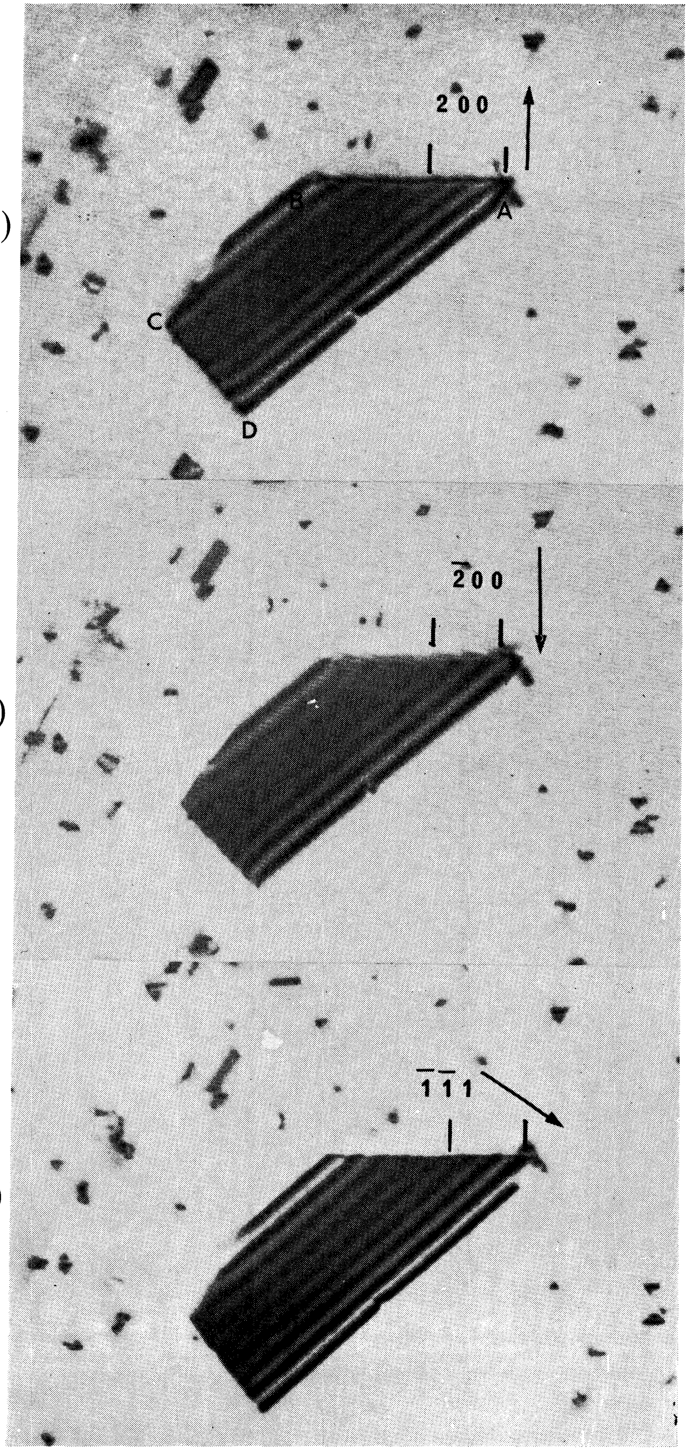

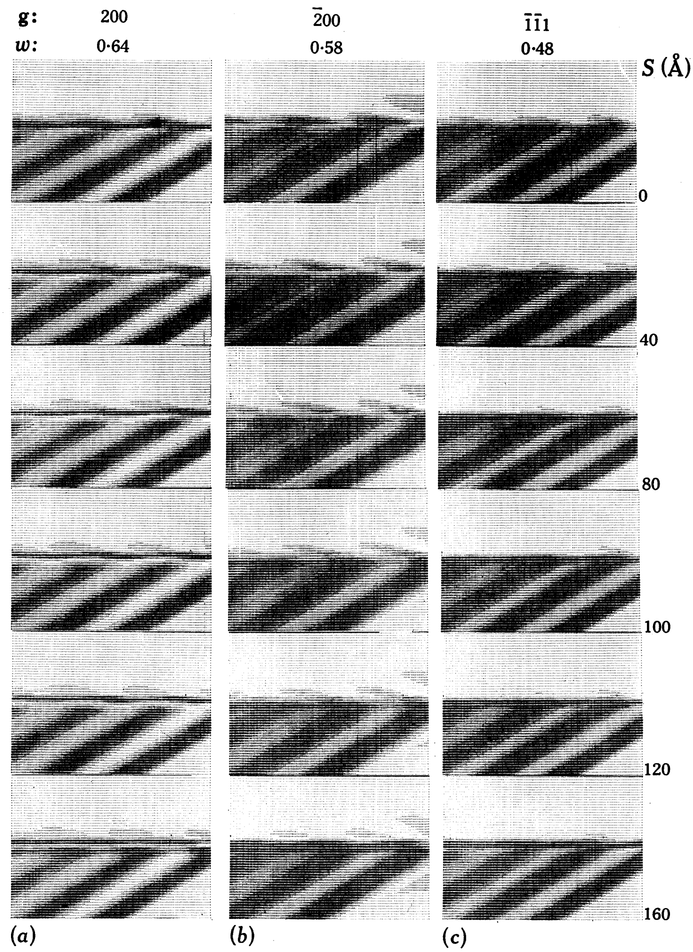

Fig. 6.—Comparison of experimental (*opposite*) and computed (*above*) images for the edge AB of a Frank dislocation loop in a copper–aluminium (9·4 at.%) alloy ($\times 60\,000$):

$$\boldsymbol{B}\ [011], \quad \boldsymbol{FN}\ [247], \quad \boldsymbol{u}\ [0\bar{1}1], \quad t = 7\xi_{200}.$$

The portions of the experimental images corresponding to the computed images are marked. The values of S, $\boldsymbol{g}$, and w are indicated. Line resolution is 29 Å.

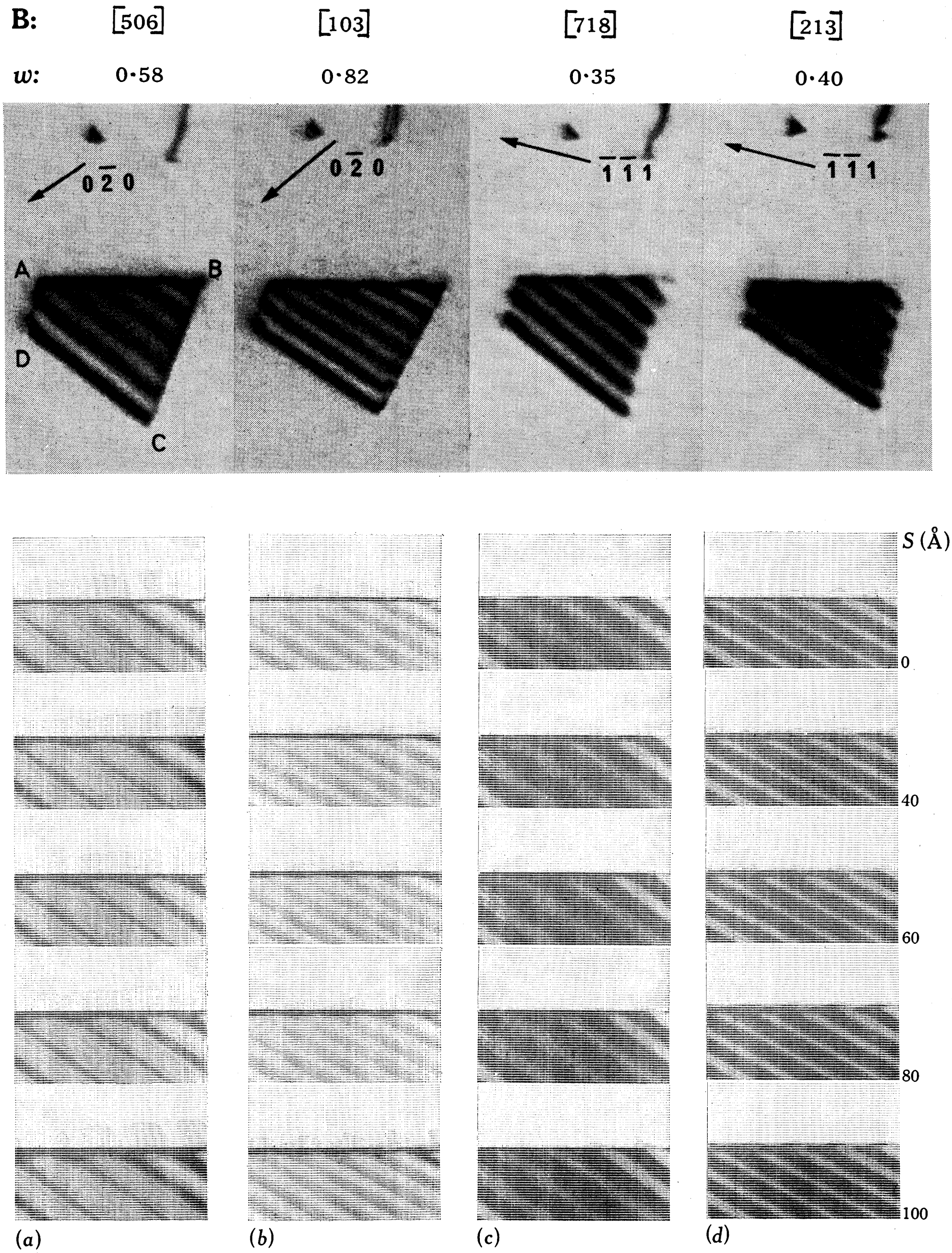

Fig. 7.—Comparison of experimental (×120 000) and computed images for the edge AB of a Frank dislocation loop in a copper–aluminium (9·4 at.%) alloy:

$$\boldsymbol{FN}\ [7\,\bar{1}\,10],\qquad \boldsymbol{u}\ [110],\qquad t = 7\xi_{200}.$$

The values of S, $\boldsymbol{B}$, $\boldsymbol{g}$, and w are indicated. Line resolution is 30 Å.

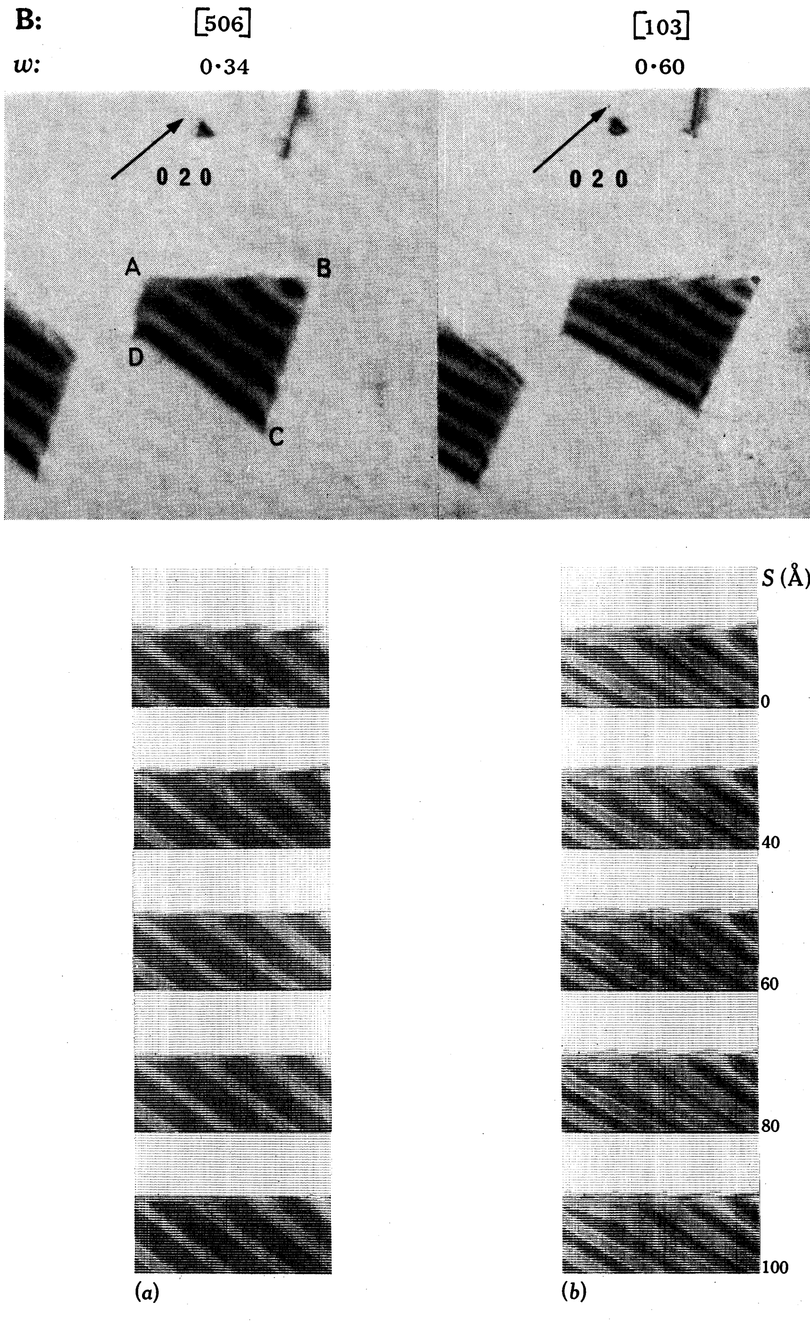

Fig. 8.—Comparison of experimental ($\times$ 120 000) and computed images for the edge AB of a Frank dislocation loop in a copper–aluminium (9·4 at.%) alloy:

$$\boldsymbol{FN}\ [7\,\bar{1}\,10], \quad \boldsymbol{u}\ [110], \quad t = 7\xi_{200}.$$

The values of S, $\boldsymbol{B}$, $\boldsymbol{g}$, and w are indicated. Line resolution is 30 Å.

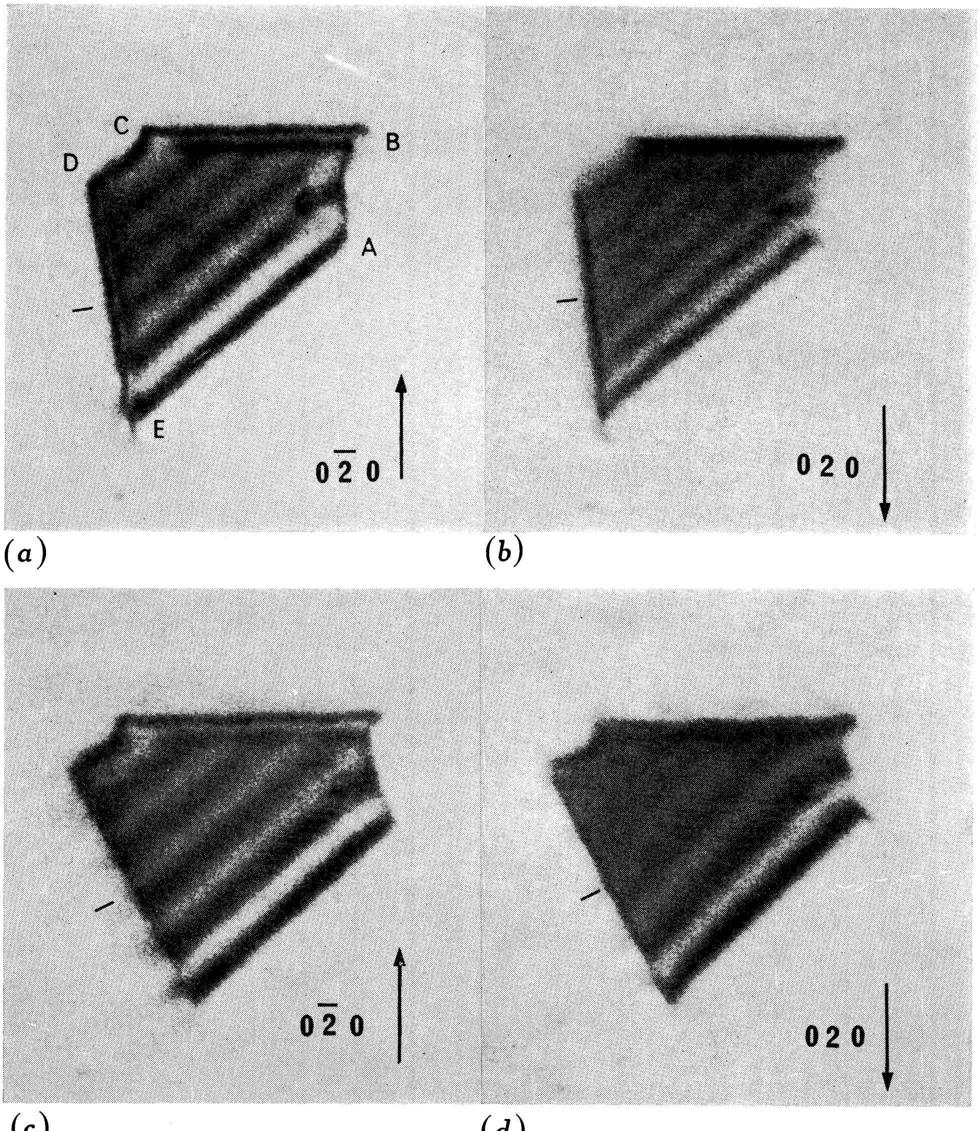

Fig. 9.—Frank dislocation loop in a copper–aluminium (15·6 at.%) alloy (×200 000):

(*a*) $\boldsymbol{B}$ [001], $\boldsymbol{g}$ $0\bar{2}0$; (*b*) $\boldsymbol{B}$ [001], $\boldsymbol{g}$ 020;

(*c*) $\boldsymbol{B}$ [102], $\boldsymbol{g}$ $0\bar{2}0$; (*d*) $\boldsymbol{B}$ [102], $\boldsymbol{g}$ 020.

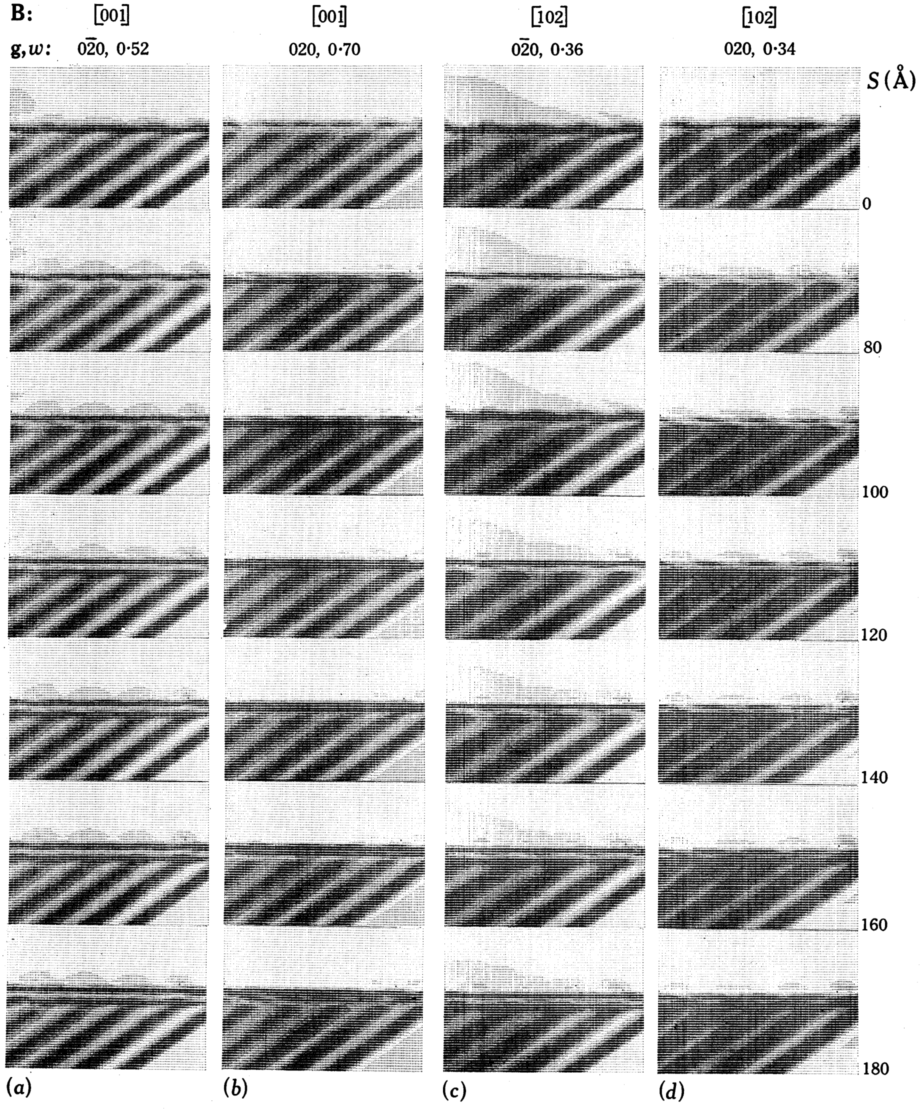

Fig. 10.—Computed images for the edge BC of the Frank dislocation loop in Figure 9:

$$\boldsymbol{FN}\ [207], \quad \boldsymbol{u}\ [\bar{1}01], \quad t = 6 \cdot 5\xi_{020}.$$

The values of S, $\boldsymbol{B}$, $\boldsymbol{g}$, and w are indicated. Line resolution is 19 Å in (*a*) and (*b*) and 25 Å in (*c*) and (*d*).

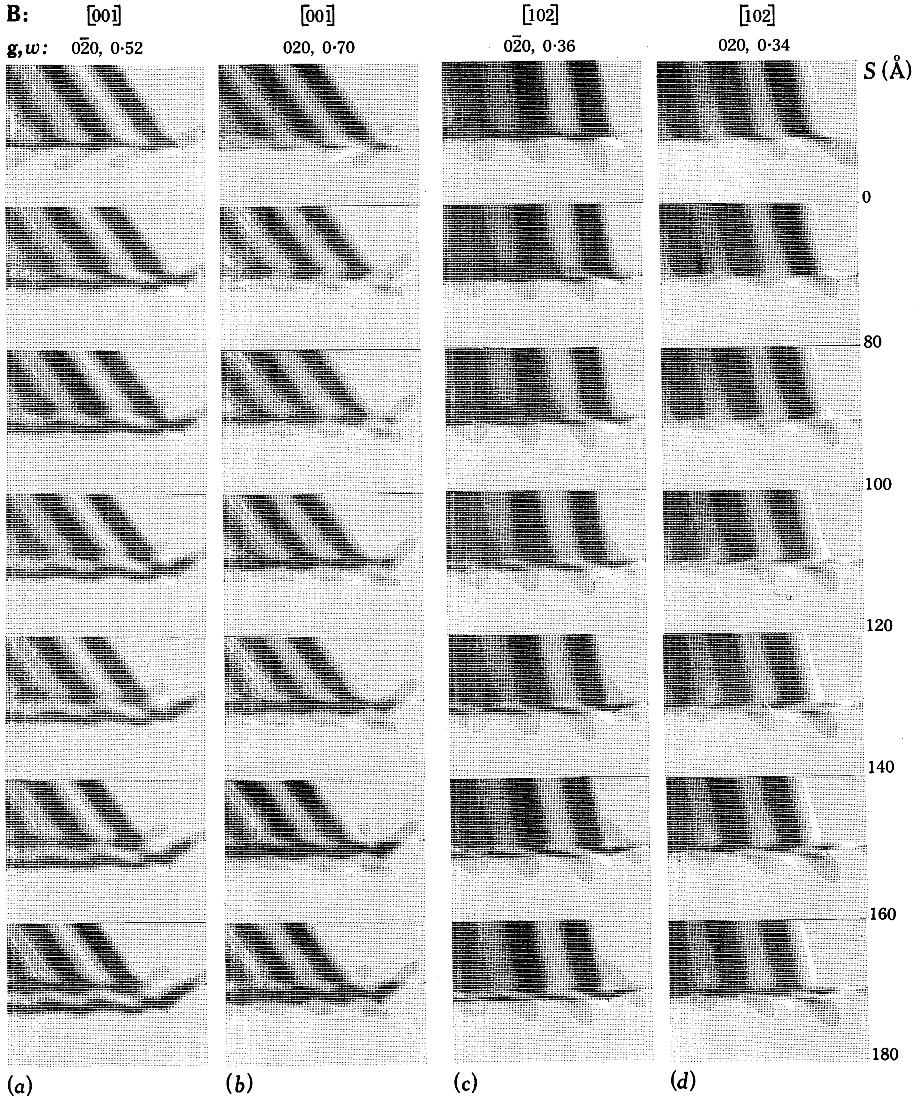

Fig. 11 (*above*).—Computed images from the surface to the marked portion of the edge DE of the Frank dislocation loop in Figure 9:

$$\boldsymbol{FN}\ [207], \quad \boldsymbol{u}\ [011], \quad t = 6\cdot 5\xi_{020}.$$

The values of S, $\boldsymbol{B}$, $\boldsymbol{g}$, and w are indicated. Line resolution is 12 Å.

Fig. 12 (*opposite*).—Comparison of experimental ($\times 60\,000$) and computed images of the marked portion of the edge AB of a Frank dislocation loop in silver:

$$\boldsymbol{FN}\ [114], \quad \boldsymbol{u}\ [\bar{1}01], \quad t = 7\xi_{020}.$$

The values of S, $\boldsymbol{B}$, $\boldsymbol{g}$, and w are indicated. Line resolution is 17 Å. The visibility limits for (*a*) and (*c*) correspond to 14% below and 25% above background.

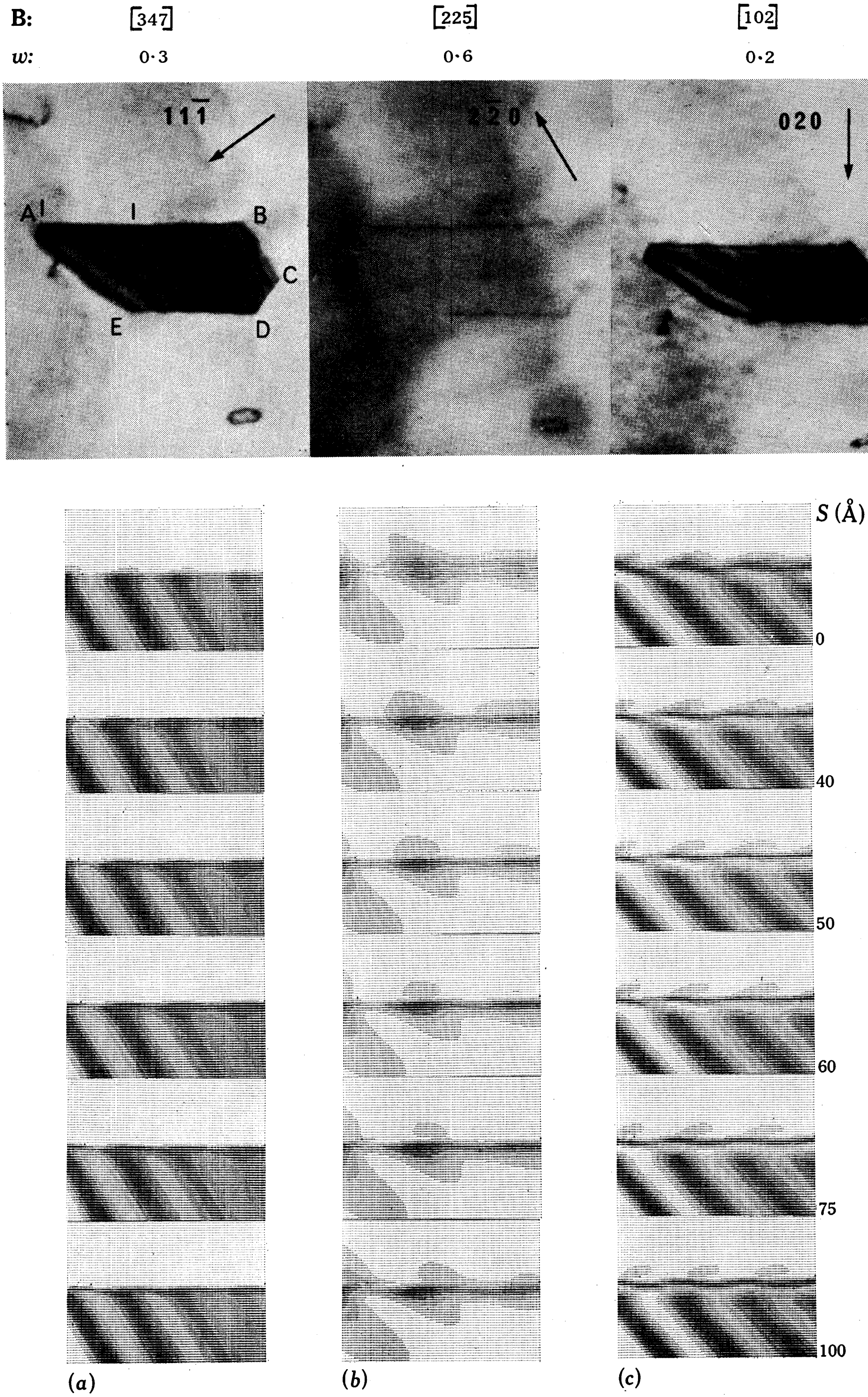
B:
[347]
[225]
[102]
w:
0·3
0·6
0·2
$11\bar{1}$
$\bar{2}20$
020
A
I
B
C
D
E
S (Å)
0
40
50
60
75
100
(a)
(b)
(c)

Fig. 12

images, the computed 020 images of the undissociated Frank are similar for the [506] and [103] beam directions (Figs 8(a) and 8(b)). As S increases for the 020 reflection, the dark contrast along AB crossing the light fringes disappears for the [506] beam direction, but remains for the [103] beam direction.* For the $\bar{1}\bar{1}1$ reflection and [213] beam direction a set of fringes on $(\bar{1}11)$ at the edge of the loop appear at $S = 80$ Å (Fig. 7(d)). It is considered that the comparison of all the experimental and computed images indicates for this edge of the loop a value of S between 60 and 80 Å.

(b) *Copper–Aluminium (15·6 at.%) Alloy*

The stacking fault energy of copper decreases with increasing concentration of aluminium (Howie and Swann 1961) so that larger separations of Shockley and stair-rod dislocations are to be expected from dissociation of Frank dislocations in the 15% aluminium alloy than in the 9·4% aluminium alloy. The 15% aluminium alloy has not been studied as extensively as the 9·4% one but, in general, the contrast effects at the edges of Frank dislocation loops, though similar to those for the 9·4% alloy, suggested a greater extent of dissociation.

Figure 9 shows an example of a Frank loop in this alloy which is of particular interest since the contrast reverses for two edges of the loop in 020 and $0\bar{2}0$ reflections, but not for the other two. The loop ABCDE lies on $(1\bar{1}1)$ and intersects the top of the foil along AE. The edge BC is along $[\bar{1}01]$ and the edge DE along [011]. The other two edges AB and CD do not lie along $\langle 110 \rangle$ directions. Comparison of Figures 9(a) and 9(b) shows reversal of contrast for the edges AB and CD on changing the operative reflection from $0\bar{2}0$ to 020, whereas the edges BC and DE show strong contrast for both reflections.

For the [001] beam direction, the contrast along BC for the $0\bar{2}0$ reflection consists of two continuous strong dark lines separated by a light band, whilst that along DE consists of a strong continuous dark line at the edge of the loop separated by a light band from an inner line which shows accentuated contrast at the ends of the dark fringes (Fig. 9(a)). For the 020 reflection, the images along BC and DE consist of broad single dark lines (Fig. 9(b)).

For the [102] beam direction, the image along BC for the $0\bar{2}0$ reflection is similar to that in the [001] beam direction, but the inner of the two dark lines is less continuous, whilst the image along DE is very weak, particularly near the surface of the foil (Fig. 9(c)). For the 020 reflection, the image along BC shows some resolution into a double image with the inner line more intense than the outer, whilst the image along DE, although not as intense as for the 020 reflection in the [001] beam direction, is stronger than that for the $0\bar{2}0$ reflection in [102] (Fig. 9(d)).

Thus we have here a case where dislocations at the edges of a faulted loop show equally strong contrast for $0\bar{2}0$ and 020 reflections in the [001] beam direction and an example where the contrast for one of these edges is stronger for the 020 reflection than for $0\bar{2}0$ reflection on rotation to the [102] beam direction. For an undissociated dislocation the $0\bar{2}0$ reflection corresponds to $\boldsymbol{g}.\boldsymbol{b} = +\frac{2}{3}$ and the 020 reflection to $\boldsymbol{g}.\boldsymbol{b} = -\frac{2}{3}$.

* The absence of the thin dark streaks of contrast crossing the light fringes at $S = 80$ Å is due to inadequate resolution in this computed image. Images computed at a higher magnification show that these dark streaks, although very fine, are still present.

Dissociation of Frank dislocations along BC and DE will give overlapping stacking faults that overlap equally in the [001] beam direction. However, on rotation to the [102] beam direction, the extent to which the faults overlap for $\boldsymbol{u}$ along [011] (edge DE) will decrease, whilst it will remain unchanged for $\boldsymbol{u}$ along $[\bar{1}01]$ (edge BC). That the contrast effects in Figure 9 are due to dissociation of Frank dislocations along BC and DE is confirmed from a comparison of the experimental images with the computed images in Figure 10, for edge BC, and Figure 11, for edge DE. The fact that the edges AB and CD are in and out of contrast for the $0\bar{2}0$ and 020 reflections respectively in the [001] beam direction suggests that they are Frank dislocations that have not dissociated to any extent and this is compatible with the fact that they do not lie along $\langle 110 \rangle$.

It is clear that the computed images for the undissociated Frank dislocations do not match the experimental images and it is considered that the detail of the experimental images is best matched by the computed images at a separation of the Shockley and stair-rod dislocations of approximately 140–160 Å.

(c) *Silver*

Frank loops observed in quenched pure silver also exhibit contrast effects associated with dissociation of the Frank dislocation (Part I). The loop shown in Figure 12 lies on (111) and intersects the bottom foil surface along AE. The loop edge AB lies along $[\bar{1}01]$ so that dissociation along this edge would occur on $(1\bar{1}1)$.

For the $11\bar{1}$ reflection, there is strong contrast along all edges except BC for which $\boldsymbol{g}.\boldsymbol{u} = 0$. Further, for the $2\bar{2}0$ reflection the image along those edges with $\boldsymbol{u}$ not parallel to $\boldsymbol{g}$ is continuous and single, whereas for BC ($\boldsymbol{g}$ parallel to $\boldsymbol{u}$) no contrast is observed. The prominent feature of the image for the 020 reflection is the light band separating the fault fringes from the line of strong contrast along edges AB and DE for which $\boldsymbol{g}.\boldsymbol{u} = 0$.

Computed images for undissociated and dissociated Frank dislocations along AB are given in Figure 12. It is clear that the computed images of the undissociated Frank dislocation do not match the observations. It is considered that a value of S between 60 and 75 Å is needed to match the continuous light band for the 020 reflection, the continuous $2\bar{2}0$ image, and the strong contrast at the edge of the loop for the $11\bar{1}$ reflection.

IV. Discussion

The agreement between the experimental images in the copper–aluminium alloys and in silver and those computed for the experimentally determined constants, on the assumed dissociated model, shows that the edges of the Frank dislocation loops in these materials are dissociated.

In the model used for the computations, the Shockley and stair-rod dislocations are straight and parallel over their entire length and as expected, no contrast is obtained in a computed image when $\boldsymbol{g}$ is parallel to $\boldsymbol{u}$. The good agreement obtained between the experimental and the computed images close to obtuse corners and at surface intersections is surprising, since the dissociation model used here cannot take into account changes in the configuration of the dislocations at such sites and no allowance is made for surface relaxation in the computations.

The equilibrium separation of the Shockley and stair-rod dislocations due to dissociation of a Frank dislocation is controlled by the stacking fault energy γ. Since the dislocations are in edge orientation, their equilibrium separation r in an elastically isotropic material is given by (Read 1953)

$$r = Gb^2(2+\nu)/36\pi\gamma(1-\nu)\,, \tag{1}$$

where G is the shear modulus, b is the closest distance of approach of the atoms, and ν is Poisson's ratio.

TABLE 1

VALUES OF γ/Gb FOR VARIOUS EQUILIBRIUM SEPARATIONS OF SHOCKLEY AND STAIR-ROD DISLOCATIONS

Separation (Å)	Silver	$(\gamma/Gb)\times 10^3$ Copper–Aluminium (9·4 at.%)	Copper–Aluminium (15·6 at.%)
40	2·90		
50	2·32		
60	1·94	1·70	
70	1·66	1·45	
80	1·45	1·27	
90		1·13	
100		1·02	
120			0·85
140			0·73
160			0·64
180			0·57
200			0·51

In principle, if the separation of the Shockley and stair-rod dislocations can be determined from details of the diffraction contrast, it should be possible to determine the stacking fault energy of the material. However, this involves the assumption that the measured separation S is equal to the equilibrium separation. Values of γ/Gb for silver and the two copper–aluminium alloys corresponding to various equilibrium separations of the Shockley and stair-rod dislocations are given in Table 1. In calculating the values for silver, the values of ν used are those given by Teutonico (1967) as effective for a {111} plane, and similar values for copper–aluminium were calculated from the equations of Aerts *et al.* (1962) (equations 7 in Teutonico 1967), using the single crystal elastic constants given in Section II (*c*).

For silver, the details of the contrast described in Section III (*c*) suggest a separation of Shockley and stair-rod dislocations of 60 Å, which leads to a value of $\gamma/Gb = 1\cdot 94\times 10^{-3}$, in reasonable agreement with previous estimates from node measurements (cf. for example, Loretto, Clarebrough, and Segall 1964). For the copper–aluminium alloys, matching between the experimental and theoretical images was obtained at different values of separation for the different alloys. For the $9 \cdot 4$ at.% alloy the results suggest a separation of 60–80 Å. The cases considered for the $15 \cdot 6$ at.% alloy indicate separations of 140–160 Å, and thus a decrease in γ/Gb with increasing concentration of aluminium. Estimates of γ/Gb for the two compositions of copper–aluminium alloy used here can be made from the measurements of node radii in this system by Howie and Swann (1961) after increasing their values of γ/Gb by the factor $2 \cdot 3$ recommended by Brown (1964). Howie and Swann's data then indicate a value of γ/Gb for the $9 \cdot 4$ at.% alloy of $1 \cdot 29 \times 10^{-3}$ and for the $15 \cdot 6$ at.% alloy of $0 \cdot 53 \times 10^{-3}$. These values are in reasonable agreement with separations of Shockley and stair-rod dislocations of approximately 70 Å in the $9 \cdot 4$ at.% alloy and 160 Å in the $15 \cdot 6$ at.% alloy.

The difficulty in applying the present method to determining stacking fault energy comes from the assumption $S = r$. Stress in the thin foil may influence the separation of the Shockley and stair-rod dislocations in a pure metal and stress, lattice friction, and segregation may influence the separation in alloys. The influence of lattice friction and/or segregation in the alloy could possibly be taken into account by comparing details of the contrast before and after annealing treatments (Swann 1964).

Since it is likely that the present method of estimating γ/Gb would still be applicable at values of γ/Gb for which nodes are too small to measure, it would be of interest to examine Frank dislocation loops in pure metals of higher stacking fault energy, such as gold, copper, and nickel, to determine whether smaller extents of dissociation can be estimated from fine details of the images.

V. Acknowledgments

We are indebted to Dr. P. Humble for the use of his computer programme, which he developed to treat problems of the type investigated here, and to him and Dr. A. K. Head for many helpful discussions. We are extremely grateful to Mr. E. G. Beckhouse for photographic work.

VI. References

Aerts, E., Delavignette, P., Siems, R., and Amelinckx, S. (1962).—*J. appl. Phys.* **33**, 3078.
Brown, L. M. (1964).—*Phil. Mag.* **10**, 441.
Hashimoto, H., Howie, A., and Whelan, M. J. (1962).—*Proc. R. Soc.* A **269**, 80.
Hearmon, R. F. S. (1956).—*Adv. Phys.* **5**, 323.
Hirsch, P. B., Howie, A., Nicholson, R. B., Pashley, D. W., and Whelan, M. J. (1965).—"Electron Microscopy of Thin Crystals." p. 496. (Butterworths: London.)
Howie, A., and Swann, P. R. (1961).—*Phil. Mag.* **6**, 1215.
Humble, P. (1968).—*Aust. J. Phys.* **21**, 325.
Loretto, M. H. (1965).—*Phil. Mag.* **12**, 125.
Loretto, M. H., Clarebrough, L. M., and Segall, R. L. (1964).—*Phil. Mag.* **10**, 731.
Mazey, D. J., Barnes, R. S., and Howie, A. (1962).—*Phil. Mag.* **11**, 459.
Read, W. T. (1953).—"Dislocations in Crystals." p. 131. (McGraw-Hill: New York.)
Swann, P. R. (1964).—*Discuss. Faraday Soc.* **38**, 84.
Teutonico, L. J. (1967).—*Phil. Mag.* **15**, 959.